ELSEVIER

Carbohydrate Research 313 (1998) 91–105

CARBOHYDRATE RESEARCH

Cyclofructins with six to ten β-(1→2)-linked fructofuranose units: Geometries, electrostatic profiles, lipophilicity patterns, and potential for inclusion complexation[1]

Stefan Immel, Guido E. Schmitt, Frieder W. Lichtenthaler *

Institut für Organische Chemie, Technische Universität Darmstadt, Petersenstraße 22, D-64287 Darmstadt, Germany

Received 7 June 1998; accepted 24 July 1998

Abstract

Cyclofructins composed of six (**1**, "CF_6") to ten (**5**, "CF_{10}") β-(1→2)-linked fructofuranose units were subjected to conformational analysis using Monte Carlo simulations based on the PIMM91 force-field. Breaking the molecular symmetry partially by alternating inclination of the *spiro*-type anellated fructofuranoses relative to the crown ether ring core, i.e. the 3-OH groups pointing either towards or away from the molecular center, substantially lowers the strain energy of the cyclofructins. The global energy-minimum geometries of CF_6, CF_8, and CF_{10} exhibit $C_{n/2}$ rotational symmetry, whilst the odd-membered macrocycles in CF_7 and CF_9 adopt C_1 symmetry. Identical conformations of the solid-state geometry of CF_6 (**1**) and its computer-generated form manifest the reliability of the computational analysis. The molecular surfaces calculated for the energy-minimum structures establish a disk-type shape for CF_6 (**1**), CF_7 (**2**), and CF_8 (**3**), whereas further ring enlargement to CF_9 (**4**) and CF_{10} (**5**) leads to torus-shaped molecules with through-going cavities. Color-coded projection of the molecular lipophilicity patterns (MLPs) and the electrostatic potential profiles (MEPs) onto these surfaces cogently displays the crown ether-like properties, favoring the complexation of metal cations via strong electrostatic interactions through the 3-OH groups located on the hydrophilic molecular side. The central cavities of CF_9 and CF_{10} are characterized not only by significantly enhanced hydrophobicity, but also by highly negative electrostatic potentials around the narrow aperture of the tori made up by the 3-OH/4-OH groups, and positive potentials on the opposite rim. Accordingly, CF_9 and CF_{10} are capable to form inclusion complexes, the cavity of the latter being approximately as large as the one of α-cyclodextrin. Calculation of the inclusion complex geometries of CF_9 with β-alanine and of CF_{10} with *p*-aminobenzoic acid revealed the guest to be deeply incorporated into the respective cavities, masking the guest's hydrophobic parts. Analysis of the electrostatic interactions at the interface of the zwitter-ionic guests with the oppositely polarized hosts predicts a high degree of regiospecificity for complex formation.

* Corresponding author. Fax: +49-6151-166674; e-mail: fwlicht@sugar.oc.chemie.tu-darmstadt.de

[1] Molecular modeling of saccharides, Part 19. For Part 18, see ref. [1].

0008-6215/98/$—see front matter
PII S0008-6215(98)00208-0

Keywords: Cyclofructins, molecular geometries of; Molecular modeling; Lipophilicity patterns; Electrostatic potential profiles; Inclusion complexation, capability for

1. Introduction

Exposure of inulin, a polysaccharide made up of β-(1→2)-linked fructofuranose residues, to digestion with a *Bacillus circulans*-derived [2] fructosyltransferase not only leads to the generation of linear oligosaccharides, but to a number of cyclic ones, namely those containing six (**1**), seven (**2**), and eight (**3**) fructofuranose units [3,4]. In line with the simplified nomenclature recently proposed [5] for cyclooligosaccharides composed of sugar units other than glucose, **1** is designated a cyclo-β-(1→2)-fructohexaoside or α-cyclofructin [5,6], thereby alluding to its analogy to α-cyclodextrin which is similarly composed of six sugar (glucose) units. Correspondingly, the higher homologs could be termed β- and γ-cyclofructin[2] which becomes impractical, however, when further increasing the number of fructose units in the macrocycle. Thus, we here propose and use the abbreviated designation CF_6 for **1**, and CF_7 to CF_{10} for the next larger ones, i.e., **2–5**, respectively (Scheme 1).

In the solid state [21], the cyclohexamer **1** (CF_6) possesses a unique 18-crown-6 skeleton as the central core, onto which the furanoid rings are *spiro*-anellated in a propeller-like fashion, pointing alternatively in opposite directions with respect to the plane of the macrocycle. Computation of the contact surface of **1** [6] revealed a disk-shaped molecular geometry with shallow central indentations on either side, thus precluding the formation of cyclodextrin–analog inclusion complexes which would require a "through-going" cavity. As the lipophilicity pattern of **1** shows a distinct "front/back"-differentiation of hydrophilic and hydrophobic surface regions [6], sandwich-type guest–host interactions appear conceivable, i.e., encapsulation of a neutral molecule by two cyclofructin disks. Whilst these have as of now not been detected, the cyclofructins **1–3** are capable of complexing metal cations in decreasing affinity $CF_6 > CF_7 > CF_8$ [22]. Therefrom, Ba^{2+} evolved as a favorably predisposed match for the CF_6, obviously due its propitious nestling in or rather above the central indentation of **1** [23]—a behavior that can be rationalized on the basis of the Molecular Electrostatic Potential (MEP) profile on the contact surface, which reveals one side of **1** to have distinctly electropositive central surface regions, whilst the other is as pronouncedly electronegative [6]. Interestingly, the preference for Ba^{2+} binding

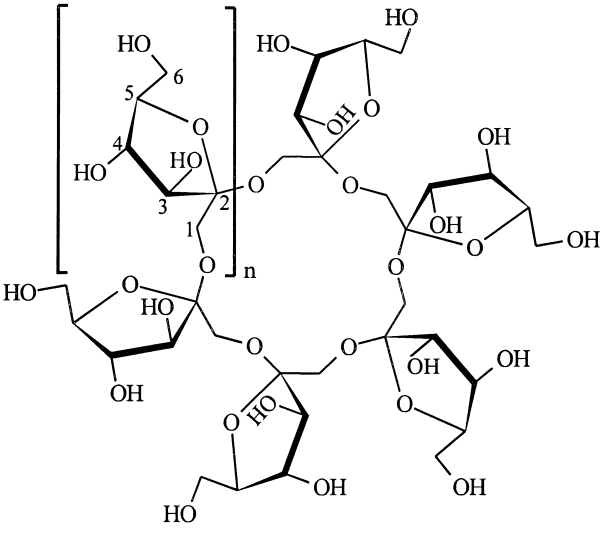

1	*cyclo*[D-Fru*f*-β-(1→2)-]$_6$	(CF_6)
2	*cyclo*[D-Fru*f*-β-(1→2)-]$_7$	(CF_7)
3	*cyclo*[D-Fru*f*-β-(1→2)-]$_8$	(CF_8)
4	*cyclo*[D-Fru*f*-β-(1→2)-]$_9$	(CF_9)
5	*cyclo*[D-Fru*f*-β-(1→2)-]$_{10}$	(CF_{10})

Scheme 1.

[2] For designating higher homologs of cyclooligosaccharides, e.g., the various cyclodextrins available today ranging from five [7] to several hundred [8] glucose residues in the macrocycle, it becomes inopportune to differentiate them by letters of the Greek alphabet. It is inconvenient, for example, to assign an appropriate letter to the cyclo-α-(1→4)-glucopentaoside, which has not only been shown by molecular modeling to be viable [9], but has yielded to synthesis [7]; the abbreviated designation "CD_5" appears not only simpler but practical. In a similar fashion, it would be advisable to abandon Greek letters for designating large-ring CDs, as the last to be named this way (ω-CD) would be the one having 29 glucose units; by contrast, the acronym "CD_{29}" is considerably more lucid and comprehensible. Accordingly, the already known δ- [10], ε- [11–13], ζ- [11], η- [14], θ- [11], ι- [13,15], λ- [15], and μ-cyclodextrins [15] are more comprehensively referred to as CD_9 through CD_{17}, respectively; similarly a "cyclomaltooctadecaose" [16], "cyclomaltononadecaose" [16], and the "cyclomaltooligosaccharide of dp 21" [17] are preferably abbreviated as CD_{18}, CD_{19}, and CD_{21}. The recent use of the cycloamylose-derived abbreviation "CA" for higher cyclodextrin homologs [13,17] appears unfortunate, as this acronym should be reserved for the cycloaltrins that have recently become accessible, i.e., CA_6 [18], CA_7 [19], and CA_8 [20].

is even more pronounced in the per-*O*-methylated α-cyclofructin [23].

Thus, in a rather unique way, cyclofructins of type **1–3** combine crown ether-type metal complexation with the capability for lipophilicity-mediated guest–host interactions, which are expected to become more dominant on increasing the ring size, i.e., on enlarging the central dents to pockets and eventually to through-going cavities. As these potentialities could open up new molecular recognition patterns in the cyclooligosaccharide field, we have deemed it of interest to extend our molecular modeling—confined to the hexamer **1** as of now [6]—to the higher homologs with seven to ten fructofuranose units. The results presented here provide a clear description of their molecular geometries, their MEP and MLP profiles, and, for CF_9 (**4**) and the decamer CF_{10} (**5**) a first assessment of their capabilities to form inclusion compounds.

2. Results and discussion

As the global geometries, molecular shapes, and the total molecular conformational energies of the cyclofructins mainly depend on the backbone torsion angles Φ, Ψ, and Θ, as well as on the propeller angles ζ of the fructose units that directly denote their inclinations towards the mean plane of the macrocycle (cf. Fig. 1), these parameters were determined by PIMM91 force-field mediated [24] Monte Carlo (MC) calculations and unrestricted "random-walk" simulations [25] using adapted corner-flapping procedures [26]. Thereby, the respective starting geometries for **1–5** were derived from the solid-state structure of CF_6-trihydrate (**1**·3 H_2O) [21] by assembling two different fructofuranosyl geometries of the asymmetric unit to symmetrical and asymmetrical macrocycles. Out of a total of approximately 130000 structures optimized for each of the cyclofructins, the global energy-minimum geometries were determined [27]; their individual parameters are listed in Table 1. The corresponding molecular conformations are displayed in Fig. 2 in the form of ball-and-stick models, onto which their MOLCAD program-generated [28] contact surfaces [29,30] were superimposed. All cyclofructins emerge as essentially unstrained macrocycles of disk- (**1, 2**, and **3**) or torus–type shape (**4** and **5**), with the primary 6-CH_2OH

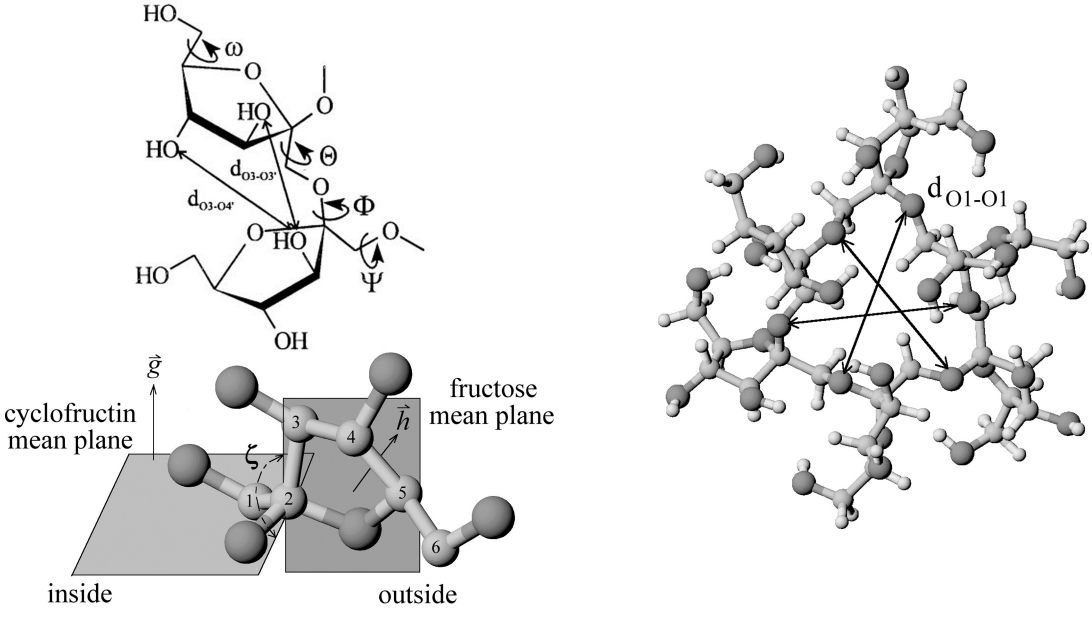

Fig. 1. Cyclofructin geometry descriptors: the torsion angles describing the conformations of the crown ether backbone are denoted as Φ (C-1–C-2–O-1′–C-1′), Ψ (C-2–O-1′–C-1′–C-2′), and Θ (O-1–C-1–C-2–O-1′); the exocyclic torsion angle ω (O-5–C-5–C-6–O-6) describes the orientation of the primary 6-OH group relative to the furanoid ring. The 3-O···O-3′– and 3-O···O-4′– interresidue distances are displayed as $d_{O3\text{–}O3'}$ and $d_{O3\text{–}O4'}$ (top left). The propeller angle ζ denotes the inclination of the furanose rings towards the macrocycle of the crown ether backbone. It is defined as the angle of the least-squares best-fit mean plane through the five furanoid ring atoms (C-2–C-3–C-4–C-5–O-5, bottom left; hydrogen atoms omitted for clarity) versus the mean plane through all backbone oxygen (O-1) atoms, i.e., the angle between the normal vectors ***g*** (pointing towards the 3-OH/4-OH side of the furanoid rings) and ***h*** (pointing in direction of a clockwise view on C-2–C-5 and O-5). Values of $\zeta \approx 90°$ indicate a perpendicular orientation of both planes. The atomic distances between the crown ether backbone oxygens (O-1) diagonally across the macrocyclic ring are denoted as $d_{O1\text{–}O1'}$ (right).

Table 1
Mean molecular geometry parameters as defined in Fig. 1 of the calculated cyclofructin structures (PIMM91) with six (**1**, CF_6), seven (**2**, CF_7), eight (**3**, CF_8), nine (**4**, CF_9), and ten (**5**, CF_{10}) fructose units in $\beta(1\rightarrow2)$-linkages; root-mean-square (RMS) deviations in parentheses. The data derived from the crystal structure of **1** are included for comparison.

Cyclofructins		CF_6 (**1**, *crystal*)	CF_6 (**1**)	CF_7 (**2**)	CF_8 (**3**)	CF_9 (**4**)	CF_{10} (**5**)
n-Fold Rotational symmetry		C_3	C_3	C_1	C_4	C_1	C_5
Furanoid ring conformation[a]		E_3 ($\rightarrow{}^4T_3$)	E_3 ($\rightarrow{}^4T_3$)	E_3 ($\rightarrow{}^4T$)	${}^4T_3$ ($\rightarrow E_3$)	${}^4T_3$ ($\rightarrow E_3$)	${}^4T_3$ ($\rightarrow E_3$)
Cremer–Pople parameters[b]	$\langle q\rangle$	0.40(0.02)	0.41(0.01)	0.43(0.02)	0.43(0.02)	0.43(0.03)	0.43(0.03)
	$\langle\phi\rangle$	260.5(1.2)	257.9(1.5)	255.0(16.0)	261.4(19.0)	266.0(6.7)	265.0(6.1)
Intersaccharidic torsion angles[c] [°]	$\langle\Phi_1\rangle$	57.1[d]	64.3(0.1)[e]	70.1(9.6)[e]	63.0(1.6)[e]	64.0(5.3)[e]	62.1(0.1)[e]
	$\langle\Phi_2\rangle$	48.2[d]	56.9(0.1)	60.9(2.2)	65.4(2.6)	64.2(0.3)	61.2(0.1)
	$\langle\Phi_3\rangle$	—[f]	—[f]	−47.3[g]	—[f]	−47.8[g]	—[f]
	$\langle\Psi_1\rangle$	177.6[d]	173.6(0.1)	176.1(3.4)	174.0(5.3)	168.2(1.9)	169.1(0.1)
	$\langle\Psi_2\rangle$	178.3[d]	−177.2(0.1)	173.8(4.2)	168.1(2.6)	158.0(4.2)	150.5(0.1)
	$\langle\Psi_3\rangle$	—[f]	—[f]	−157.7[g]	—[f]	−146.0[g]	—[f]
	$\langle\Theta_1\rangle$	163.4[d]	163.1(0.1)	173.6(7.5)	176.3(5.5)	179.6(2.5)	178.5(0.1)
	$\langle\Theta_2\rangle$	52.3[d]	40.9(0.1)	39.1(10.7)	33.2(4.7)	42.4(2.3)	56.7(0.1)
	$\langle\Theta_3\rangle$	—[f]	—[f]	179.8[g]	—[f]	−173.6[g]	—[f]
Propeller angle[c]	$\langle\zeta_1\rangle$	85.7[d]	85.5(0.1)	81.2(1.8)	86.7(8.9)	83.1(1.4)	84.5(0.1)
	$\langle\zeta_2\rangle$	113.5[d]	115.5(0.1)	117.7(2.8)	118.1(2.7)	117.5(1.1)	117.4(0.1)
O-5–C-5–C-6–O-6	$\langle\omega\rangle$	−62.1(0.5)	−62.5(0.5)	−176.3(91.9)	−33.6(94.2)	119.0(61.2)	117.6(60.9)
Atomic distances [Å]	$\langle O_1–O_{1'}\rangle$[h]	6.2[d]	6.4(0.2)	7.3(0.5)	8.2(0.8)	9.1(0.7)	10.2(0.1)
	$\langle O_3–O_{3'}\rangle$[i]	4.7(0.1)	4.8(0.1)	4.6(0.7)	5.2(0.4)	4.8(0.7)	5.1(0.2)
	$\langle O_3–O_{4'}\rangle$[i]	6.3(1.0)	6.3(1.1)	6.2(1.2)	6.5(1.3)	6.1(1.4)	6.1(1.5)
	$\langle O_4–O_{4'}\rangle$[i]	7.8(0.3)	7.9(0.3)	7.4(0.7)	7.9(0.7)	7.3(0.8)	7.6(0.2)
	$\langle O_6–O_{6'}\rangle$[i]	6.8(0.9)	6.9(0.9)	7.3(1.8)	7.8(1.8)	8.6(1.3)	8.9(1.0)
	$\langle O_3–O_{3''}\rangle$[k]	3.1[d]	3.2(0.1)	3.0(0.1)	3.4(0.4)	4.1(0.2)	4.3(0.1)
	$\langle O_3–O_{3''}\rangle$[l]	8.9[d]	9.1(0.1)	9.0(0.3)	9.0(0.2)	9.7(0.2)	8.6(0.2)

[a] Mean conformation as derived from the mean Cremer–Pople ring puckering parameters.
[b] Cremer–Pople ring puckering amplitued q (in Å) and puckering angle ϕ (in °).
[c] Φ: C-1–C-2–O-1′–C-1′; Ψ: C-2–O-1′–C-1′–C-2′; Θ: O-1–C-1–C-2–O-1′; ω: O-5–C-5–C-6–O-6; ζ: angle between the best-fit mean plane of the macrocycle (defined by all O-1 atoms) and each fructose-mean plane (atoms C-2 to C-5, and O-5). The index "1" corresponds to parameters for "*inward*" inclined fructose units with the 3-OH group pointing towards the molecular center; index "2" designates "*outward*" inclined residues (3-OH directed perpendicular to the macrocycle or away from the center axis). For the odd-membered CF_7 (**2**) and CF_9 (**4**), the index "3" denotes the single torsion between the two vicinal, abnormally parallel, "*inward*" inclined fructosyl residues; e.g., Θ_1, Θ_2, and Θ_3 occur with a ratio of 3:3:1 in **2** versus 4:4:1 in **4**.
[d] Due to C_3 symmetry of **1** in the solid-state, no root-mean-square (RMS) fluctuations are given.
[e] For the calculated structures only approximate symmetries are given, i.e., RMS values indicate the "degree of symmetry".
[f] Not defined for even-membered cyclofructins **1, 3**, and **5**.
[g] Single value for which no RMS fluctuation could be given.
[h] O-1/O-1 atomic distances diagonally across the cyclofructin ring.
[i] Atomic distances between corresponding atoms contained in adjacent fructofuranosyl residues.
[k] O-3/O-3″ distances between two adjacent, "*inward*" inclined fructose moieties in a 1,3-like relationship.
[l] Analogous to k, but for two adjacent, "*outward*" inclined units.

groups and the furanoid ring oxygens O-5 located on one side of the molecule, and the secondary 3-OH and 4-OH groups on the other.

Molecular geometries of cyclofructins **1–5**.—Despite the imposing pictorial representation of the gross molecular features of cyclofructins **1–5** in Fig. 2, the abundance of data obtained and collected in Table 1 requires a brief discussion of the various individual parameters, such as conformations of the furanoid rings, of the crown ether backbone, of the hydroxymethyl groups, the interresidue distances, and the over-all dimensions.

Fructofuranose conformation. Although two different fructofuranosyl units can be distinguished on the basis of the macrocyclic crown ether backbone torsion angles, the fructofuranose ring conformations do not differ significantly in terms of the Cremer–Pople ring puckering parameters $<q>$ and $<\phi>$ [31]. All furanoid rings exhibit medium distortions of $q \approx 0.40$–0.45 Å (root-mean-square

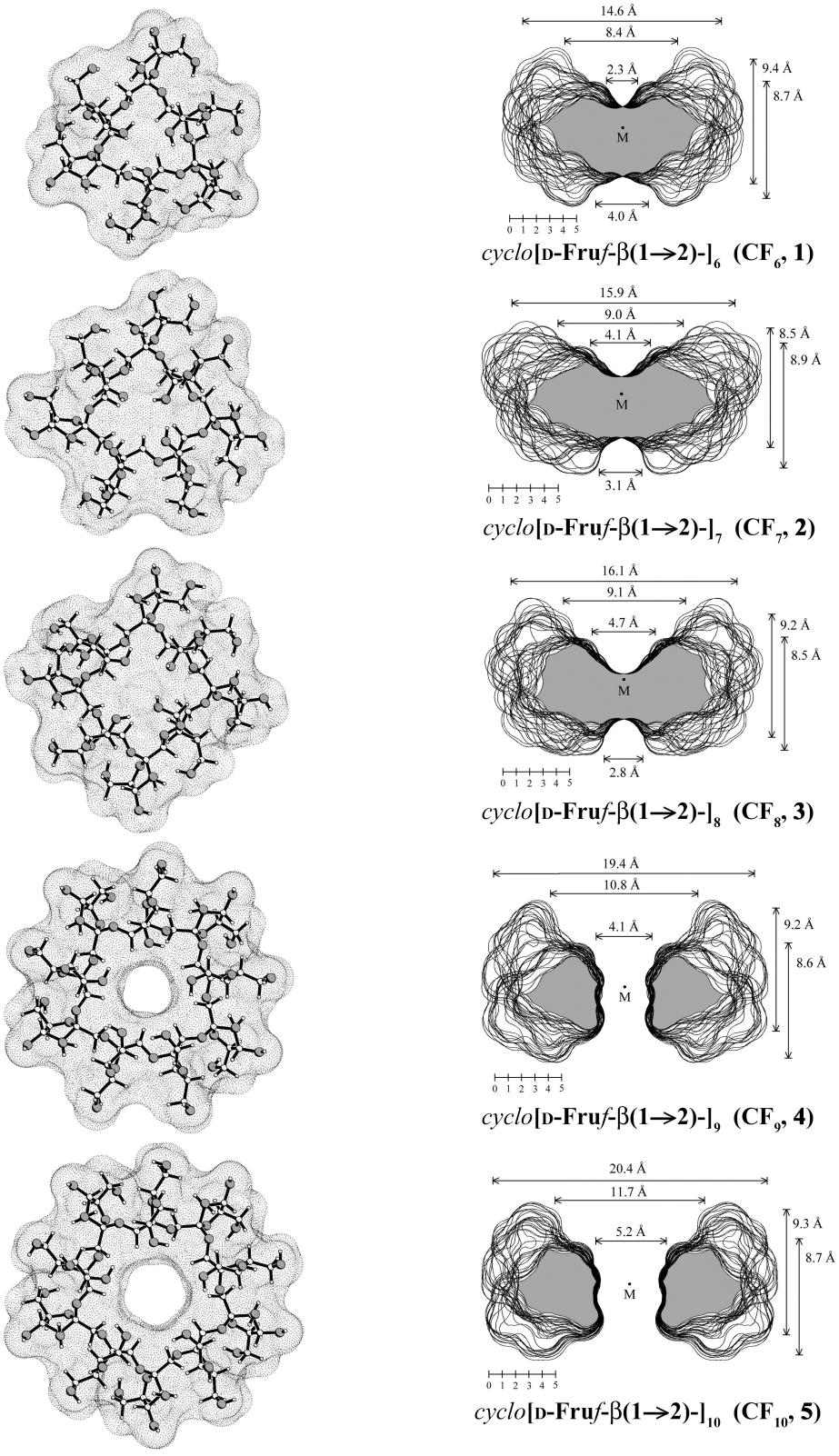

Fig. 2. Ball-and-stick model representations of the global energy-minimum geometries of the cyclofructins **1–5** with the contact surfaces superimposed in dotted form, and the corresponding cross-section plots. Structures on the left are shown perpendicular to the mean ring plane of the macrocycles; the 3-OH/4-OH side of the furanoid rings points towards the viewer, and the 6-CH_2OH groups and the 5-O atoms away from him; oxygens are shaded. Surface contours (right) were obtained for successive 10° rotation steps around the geometrical center M and superimposed. In each case the 6-CH_2OH groups are located on the top, and the 3-OH/4-OH groups on the bottom side of the models; approximate molecular dimensions are included in Å.

deviations from planarity), with the conformations uniformly being settled in the $^4T_3 \leftrightarrow E_3$ sector ($\phi \approx 255$–$265°$) of the pseudorotational itinerary for five-membered rings [32] (Fig. 3).

The orientation of the primary 6-OH groups relative to the furanoid ring, as defined by the O-5–C-5–C-6–O-6 torsion angle ω, is uniformly (−)-*gauche* in either the solid-state geometry or the PIMM91-generated form of the cyclohexamer CF_6. For the larger cyclofructins CF_7 to CF_{10}, however, no characteristic conformational preferences prevail. The very large RMS fluctuations of ω (cf. Table 1), indicate this torsion to adopt almost any value in the $-180°$ to $+180°$ range. Since the 6-CH_2OH groups are not involved in any intramolecular hydrogen bonding interactions (vide infra), they are expected to be almost freely rotatable in all compounds **1–5**.

Symmetries. Invariably, the global energy-minimum geometries of the five cyclofructins feature *n*-polygons of the O-1 atoms with average deviations from the least-squares best-fit mean plane of less than 0.20(5) Å. In fact, all Monte-Carlo simulations starting from different symmetrical structures (i.e. C_n rotational symmetry with $n = 6$–10 for **1–5**) unequivocally demonstrate one trend: "breaking" the high symmetry substantially lowers the molecular energy, i.e., the fructofuranosyl residues avoid the comparatively close spatial arrangements in the C_n symmetrical structures by diminishing steric repulsions through contra-rotatory movement of two adjacent monosaccharide units. This effect leads to an alternating "*inward*" (down) and "*outward*" (up) arrangement of the fructofuranoses relative to the mean plane of the macrocyclic backbone. As a consequence, half of the 3-OH groups (cf. Fig. 4) point towards the center of the macrocycle ("*inward*" rotation), whereas the others are situated nearly perpendicular on the ring perimeter ("*outward*" tilting).

In the even-membered cyclofructins, these conformational preferences reduce the symmetry from C_n to $C_{n/2}$, i.e., an $n/2$-fold rotational axis for CF_6 (**1**), CF_8 (**3**), and CF_{10} (**5**). Their odd-membered counterparts CF_7 (**2**) and CF_9 (**4**) cannot adopt $C_{n/2}$ symmetries a priori; however, the alternating arrangement is retained as largely as possible, with the "last" residue being "*inward*" inclined, parallel to one adjacent fructosyl unit. This arrangement reduces the backbone symmetry to C_1.

Backbone conformations. With respect to the conformations of the crown ether core of the cyclofructin macrocycles, consideration of the C-1–C-2–O-1′–C-1′ torsion angles Φ_1 (for inward inclined fructose units) and Φ_2 (for those directed towards the outside) provides the following picture: in CF_6, uniformly, an all-(+)-*gauche*-arrangement with alternating values of $\Phi_1 \approx 64.3°$ and $\Phi_2 \approx 56.9$ is adopted (cf. Table 1), in direct relation to the alternating "*inward*" and "*outward*" inclination of the fructosyl moieties (C_3 symmetry, Φ_1 as well as Φ_2 being realized thrice each). This alternating sequence is retained throughout the entire series **1–5**, with the differences between Φ_1 and Φ_2 becoming smaller with increasing ring size. However, the Φ_3 torsion angle for the "unusual" intersaccharidic linkage between the two parallel "*inward*" inclined fructofuranoses in the odd-membered cyclofructins **2** and **4**, exhibits a (−)-*gauche*-arrangement of $\approx -47°$. Analogous trends are observed for the Ψ (C-2–O-1′–C-1′–C-2′) torsion: an approximate *trans*-relationship is retained in all cases, with Ψ_1 and Ψ_2 slightly decreasing on increasing ring size of the macrocycles ($\Psi_{1/2} \approx 173.6°/-177.2°$ for CF_6, versus $\Psi_{1/2} \approx 169.1°/150.5°$ for CF_{10}). The *trans*-arrangement is also retained in Ψ_3 for CF_7 and CF_9.

The largest variations are found in the Θ (O-1–C-1–C-2–O-1′) torsion angles, which invariably adopt an alternating *trans*- ($\Theta_1 \approx 165°$–$180°$)

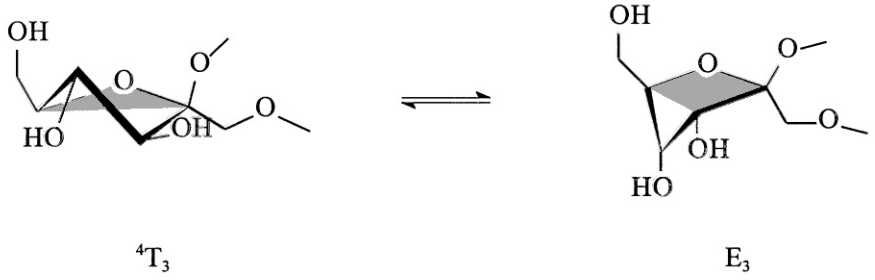

Fig. 3. Ring conformations of fructofuranose units in cyclofructins **1–5**. The orientation of the primary 6-OH relative to O-5, graphically implied here, is (−)-*gauche*, as found for the solid-state and force-field-generated geometries of CF_6 (**1**). For the larger cyclofructins no characteristic preferences prevail.

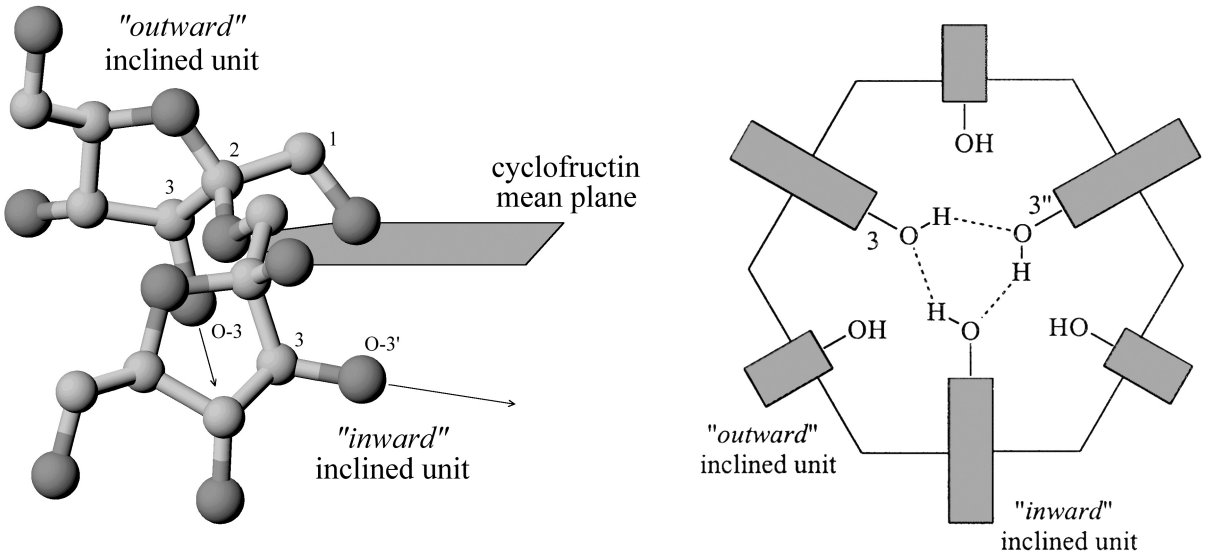

Fig. 4. Typical molecular fragment of a fructofuranosyl-β-(1→2)fructofuranose disaccharide unit. Left: Display of the alternating "*inward*" and "*outward*" inclination of the two furanoses, within the O-3 atoms pointing either towards or away from the molecular center (hydrogen atoms omitted for clarity). Right (schematic drawing): In the solid-state structure as well as in the computer-generated-form of CF_6, homodromic cycles of cooperatively strengthened intramolecular hydrogen bonds of the $[\cdots 3\text{-HO}\cdots\text{HO-}3''\cdots]_n$-type are observed between the "*inward*" inclined fructofuranose residues.

and (+)-*gauche*-sequence ($\Theta_2 \approx 35°$–$55°$) of settings. The "unusual" intersaccharidic linkages in CF_7 and CF_9 are characterized by a *trans*-relation with $\Theta_3 \approx 179.8°$ and $-173.6°$, respectively. The unique *tgtgtg*-succession of torsion angles Θ_1 and Θ_2 is not only realized in the computer-generated global energy-minimum conformation of CF_6 (**1**), but is also observed in its solid-state geometry (cf. Table 1); it must be attributed to the sterically demanding *spiro*-type anellation of furanoid rings onto the crown ether backbone as, by contrast, the unsubstituted 18-crown-6 ether crystallizes in the *gtgggt*-form [33], and its metal complexes favor *all-gauche*-arrangements [34]. The essentially identical molecular shapes and the excellent conformity of the backbone of CF_6 with its "frozen" solid-state structure also validate a previous molecular modeling study, in which only the solid-state geometry of **1** was used [6].

The propeller angle ζ indicates the inclination of the mean planes of the "*inward*" (ζ_1) and "*outward*" (ζ_2) oriented fructofuranose units towards the mean plane of the macrocycle (cf. Fig. 5 for a schematic plot of a typical molecular fragment). The observed alternating order of $\zeta_1 \approx 80$–$85°$ and $\zeta_2 \approx 113$–$118°$ establishes a "*V*"-type relationship between vicinal monosaccharide units of the cyclofructins **1–5**.

Interresidue atomic distances and hydrogen bonding. Monitoring O···O-distances on opposite faces of the macrocycles (cf. Table 1) provides a general picture of the possible types of intramolecular hydrogen-bond interactions, even if these do not actually prevail in the low–energy conformers. Whilst the distances between all combinations of O-3 and O-4 atoms are nearly constant and independent from the ring size of the cyclofructins, the O-6/O-6′ distances gradually become larger (6.9 ± 0.9 Å in $CF_6 \rightarrow 8.9 \pm 1.0$ Å in CF_{10}). Provided the O···H-length of standard hydrogen bonds to be in the range of 1.8 Å up to 2.5 Å, the limiting criterion for the corresponding O···O-distances

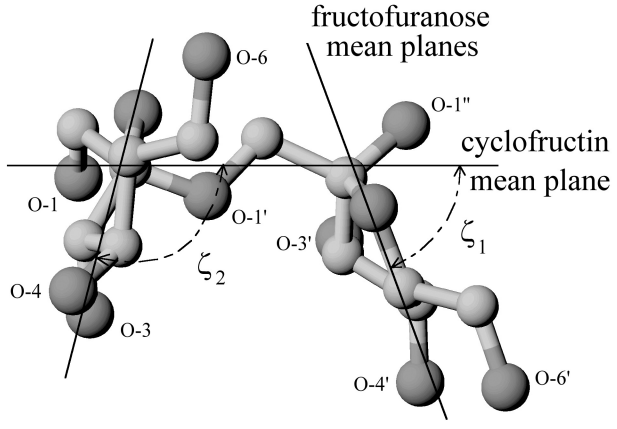

Fig. 5. Propeller angles between two fructofuranose residues as viewed from the outside of the macrocycle in the direction of its mean plane (hydrogen atoms omitted for clarity).

is a maximum of 3.5 Å. The data listed in Table 1 indicate all oxygen-oxygen distances between vicinal fructoses to be larger than 4.6 Å (up to 8.9 Å), thus prohibiting the formation of any stable intramolecular hydrogen bonds of this type. The only exception is found for the O-3/O-3′ distances between the adjacent, abnormally parallel "*inward*" inclined fructose residues in CF_7 (**2**) and CF_9 (**4**) of $\approx$ 3.4 Å and 3.1 Å, respectively. Yet, both allow for direct hydrogen bonding, albeit the 3-O···HO-3′-type bridge is realized in the computed structure of **4** only (length of H-bond $\approx$ 2.23 Å).

By contrast, the corresponding O-3/O-3″ distances for 1,3-related fructose moieties display different trends for "*inward*" or "*outward*" tilted furanoses. In the latter case, distances of >9.0 Å indicate the absence of any hydrogen bonding interaction. If both 1,3-related units are inclined "*inwards*", i.e., having their 3-OH groups directed towards the central axis of the molecule, the O-3/O-3″ distances are in the range of 3.1 Å for CF_6 and CF_7, 3.4 Å for CF_8, and $\approx$ 4.2 Å for CF_9 and CF_{10}, respectively. Thus, in CF_6 through CF_8 at least, intramolecular H-bonding networks made up by cooperatively strengthened, homodromic cycles of the type $[\cdots 3\text{-HO}\cdots\text{HO-}3''\cdots]_n$ are formed, as exemplified by the schematic drawing of CF_6 (Fig. 4, right). In fact, such an intramolecular hydrogen bond cycle is realized in the solid-state structure of CF_6.

Contact surfaces and cavity dimensions. In contrast to the almost perfectly round–shaped cyclodextrins, in which the α-(1→4)-linked glucose units are regularly and uniformly tilted towards the macrocycle [9,35], the alternating "*inward/outward*" inclination of the fructofuranosyl residues in **1–5** leaves the cyclofructins with a deeply fissured, irregular over-all shape. Cross-cut plots obtained from the intersection of a rotating plane with the cyclofructin contact surfaces (Fig. 2) clearly display a disk-type shape of **1, 2**, and **3**, versus the torus-like (doughnut) appearance of **4** and **5**; the approximate molecular dimensions displayed by these plots are listed in Fig. 2 and Table 2.

With increasing ring size, the mean macrocyclic diameters increase from approximately 14.6 Å for CF_6 (**1**), to $\approx$ 20.4 Å in CF_{10} (**5**), whilst the mean molecular height is almost constant in the range of $\approx$ 8.5–9.2 Å. The "top" and "bottom" sides of **1, 2**, and **3** are slightly indented (to an increasing extent in that order), whereas CF_9 (**4**) and CF_{10} (**5**) possess a central cavity passing through the entire molecule. In contrast to the outer shape of these macrocycles, the cavities have a nearly perfect cylinder-type appearance. The cavity radius of approx. 5.2 Å for CF_{10} (**5**) is similar to that of α-cyclodextrin (CD_6: $\approx$ 4.5–5.0 Å [5,9]), whilst the cavity of CF_9 (**4**) is substantially narrowed ($d \approx 4.1$ Å).

The wide-opened rim of the tori is made up by the 6-CH_2OH groups, the narrow rim is formed by the 3-OH and 4-OH groups, respectively.

Of the total cyclofructin surface area (cf. Table 2; $\approx$ 115–120 Å^2 per fructose unit), the cavity interior of **4** and **5** comprises $\approx$ 5–10%. The spatial volume included by the contact surfaces of **1–5** is computed to approx. 165–170 Å^3 per fructose unit. As the estimated cavity volumes of CF_9 (90 Å^3) and CF_{10} (150 Å^3) turn out to be only slightly smaller than those for the α- and β-cyclodextrins (100 Å^3 for CD_6, 160 for CD_7 [9]), similar inclusion complexations—with respect to their geometric fit— are to be expected.

Molecular electrostatic potentials (MEPs).—In view of the well-established capability of crown ethers to complex metal cations by chelate coordination and electrostatic interactions [33], we have calculated the MEP profiles of the cyclofructins **1–5** by using the MOLCAD molecular modeling program [28], whereby the relative potential values in the range of approximately −100 to +100 kJ/mol were projected in color-coded form onto the mole-

Table 2
Approximate molecular dimensions, surface extensions, and cavity characteristics of cyclofructins **1–5**

Cyclofructin	Torus diameter (Å)		Height (Å)	Surface area (Å^2)		Surface volume (Å^3)	
	Outer	Inner		Total	Cavity	Total	Cavity
CF_6 (**1**)	14.6	—	8.7–9.4	690	—	1000	—
CF_7 (**2**)	15.9	—	8.5–8.9	810	—	1180	—
CF_8 (**3**)	16.1	—	8.5–9.2	910	—	1370	—
CF_9 (**4**)	19.4	4.1	8.6–9.2	1090	90[a]	1520	90[a]
CF_{10} (**5**)	20.4	5.2	8.7–9.3	1200	115[a]	1710	150[a]

[a] Height of cavity approximately 7.0 Å.

cular contact surfaces. As imposingly set forth by the resulting color graphics (Fig. 6, left half), the 6- and 1-CH_2-groups are characterized by positive electrostatic potentials (red colors, Fig. 6 top left), with the cavity surfaces of CF_9 (**4**) and CF_{10} (**5**) being highly polarized along the molecular axis (cf. Fig. 6 bottom entries). By contrast, the opposite side made up by the negatively charged O-1, O-3, and O-4 atoms of the fructofuranoses, contributes to high negative electrostatic potentials (blue to violet colors in center entries of Fig. 6).

On the basis of the MEPs presented here, and the overwhelming NMR evidence for the complexation of the metal cations Pb^{2+}, Ba^{2+}, K^+, Rb^+, and Cs^+ by CF_6 (**1**) and CF_7 (**2**) [22,23] in aqueous solution as well as in organic solvents, it becomes obvious that the oxygen atoms O-1 and, in particular, O-3 are involved in capturing cations. The highly negative electrostatic potentials around the O-1, O-3, and O-4 atoms act as a long-range trap for cations, with repulsive positive potentials on the opposite molecular side [6]. Thus, the mechanism of complex formation must involve simultaneous or successive rotation of the *spiro*-anellated furanosyl residues to open a center pocket, whereby the resulting symmetry of the adduct depends on the strength of the Coulomb interactions (i.e., the charge of the cations) [22,23] and the preferred type of coordination.

Molecular lipophilicity patterns (MLPs).—Of the various effects that have been brought forward as the actual driving forces for host–guest complexation [36], hydrophobic interactions undoubtedly play a major role although it is exceedingly difficult to quantitatively separate hydrophobic effects [37] from the variety of binding interactions. Recently, however, we have been able to demonstrate that the molecular lipophilicity patterns (MLPs)—generated by the MOLCAD program [28] and mapped onto the respective contact surfaces [29] in color-coded form [38,39]—are a proper means to portray the hydrophobic topographies of inherently hydrophilic sugars—an approach that has provided for the first time a lucid picture of the hitherto elusive distribution of the hydrophilic and hydrophobic areas on the surface of sucrose [40,41], non-carbohydrate sweeteners [40], cyclodextrins [5,9,35] and their inclusion complexes [42], non-glucose oligosaccharides [5,18,43,44], and of the amylose portion of starch [41]. Accordingly, it was obvious to extend these studies to the cyclofructins **1–5**.

As intelligibly set forth by the color representations in Fig. 6 (right entries), the cyclofructins **1–5** exhibit a distinct differentiation of hydrophilic and hydrophobic surface regions with respect to the front and reverse sides of the disk-shaped molecules. The proximity of the 3-OH and 4-OH groups and O-1 of each fructofuranosyl moiety on the one molecular side leads to a pronouncedly hydrophilic surface area (blue areas in the half-opened models, Fig. 6, center). The molecular regions on the opposite side, however, reveal the distinctly hydrophobic character (yellow areas) around the center indentation (Fig. 6, top right), obviously originating from the 1- and 6-methylene groupings and the O-5–C-5–H-5 fragments. Clearly separated hydrophilic and hydrophobic surface areas are maintained throughout the entire series of the cyclofructins with only little changes on increasing the ring size from six to 10 fructose residues. The side view representations of the MLPs (Fig. 6, bottom) reveal the central cavities of CF_9 (**4**) and CF_{10} (**5**) to have enhanced hydrophobic character.

Inclusion complexation potential.—In the case of the disk-shaped cyclofructins CF_6, CF_7, and CF_8, the concentration of lipophilic regions on one side may—at least in the solid-state—give rise to sandwich-type guest-host interactions, i.e., a neutral guest molecule being enclosed by the hydrophobic sides of two head-to-head oriented cyclofructins. The larger ring homologs CF_9 (**4**) and CF_{10} (**5**), however, on account of their sizable cavities, are surmised to engage in cyclodextrin-like inclusion complexations. In order to gain a first notion on their capabilities to incorporate suitable guests into their cavities, the electrostatic iso-energy contour surfaces were generated. In the case of CF_{10}, for example, the dipolar character of the cavity is well embodied by the graphical presentation in Fig. 7, in which the iso-energy contours cap both ends of the cavity in a lid-like fashion, displaying an "electrostatic energy lock" that is apt to favor inclusion complex formation if oppositely polarized or even charged head groups of a guest can penetrate the low-energy regions.

Accordingly, on the basis of a mixed molecular dynamics and molecular mechanics approach (cf. Experimental) we have calculated the most stable forms of conceivable zwitterionic inclusion complexes of CF_9 with β-alanine and of CF_{10} with *p*-aminobenzoic acid. Of the two possible guest-host alignments, the ones shown in Fig. 8 are highly favored due to an opposite alignment of the

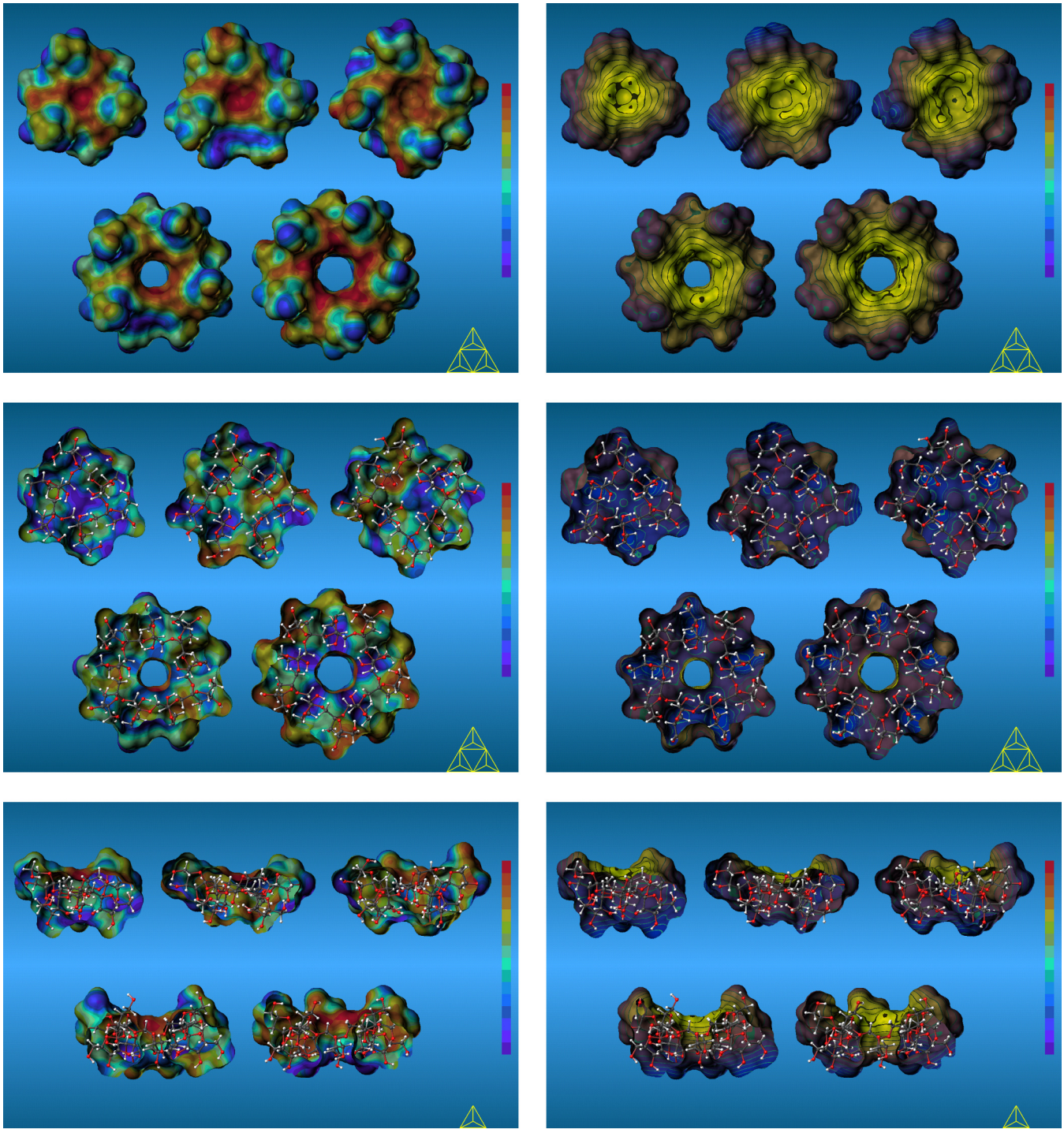

Fig. 6. MOLCAD program-generated molecular electrostatic potential profiles (MEPs, left half) and molecular lipophilicity patterns (MLPs, right half), projected onto the contact surfaces of CF_6 (**1**, upper left), CF_7 (**2**, center), CF_8 (**3**, upper right), CF_9 (**4**, lower left) and CF_{10} (**5**, lower right); molecular orientations and modes of viewing of the top and center plots are opposite to those in Fig. 2. For visualization of the MEPs (left half), a 16-color code ranging from violet (most negative potential) to red (most positive potential) is applied in relative terms for each molecule separately. The MLPs (right half) are visualized by applying a two-color code graded into 32 shades, adapted to the range of relative hydrophobicity calculated for each molecule; the 16 colors ranging from dark blue (most hydrophilic areas) to full yellow (most hydrophobic regions) are used for mapping the computed values onto the surface, whereas the remaining 16 color shades (light blue to brown) indicate iso-contour lines in between former color scale, allowing a more quantitative assessment of the relative hydrophobicity on different surface regions. The top right picture exposes the intensively hydrophobic (yellow) 1-and 6-methylene groups and the O-5–C-5–H-5-fragments of the molecules; in the center, the front half of the surfaces has been removed, providing an inside view on the hydrophilic (blue) reverse side formed by the 3-OH/4-OH side; the bisected side-view MLPs (bottom right) disclose the hydrophobic central cavities of CF_9 (**4**) and CF_{10} (**5**).

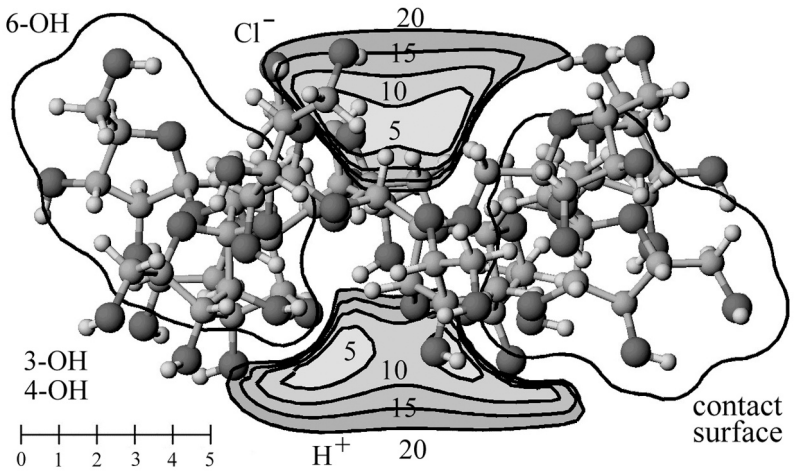

Fig. 7. Iso-energy contour surfaces for the interaction of CF_{10} (**5**) with positively (H^+) and negatively (Cl^-) charged probe spheres; energy contours are given at levels of +5.0, +10.0, +15.0, and +20.0 kJ/mol relative to the global energy minimum. On low-energy levels, these volumes designate favorable interactions with cations and anions, or partially positively and negatively charged groups of guest molecules, respectively. The side-view orientation of **5** corresponds to Figs. 2 and 6, with the 3-OH and 4-OH pointing down versus an upward direction of the 5-O and 6-CH_2OH groups. The contact surface is superimposed onto the contours and sliced through the center of geometry.

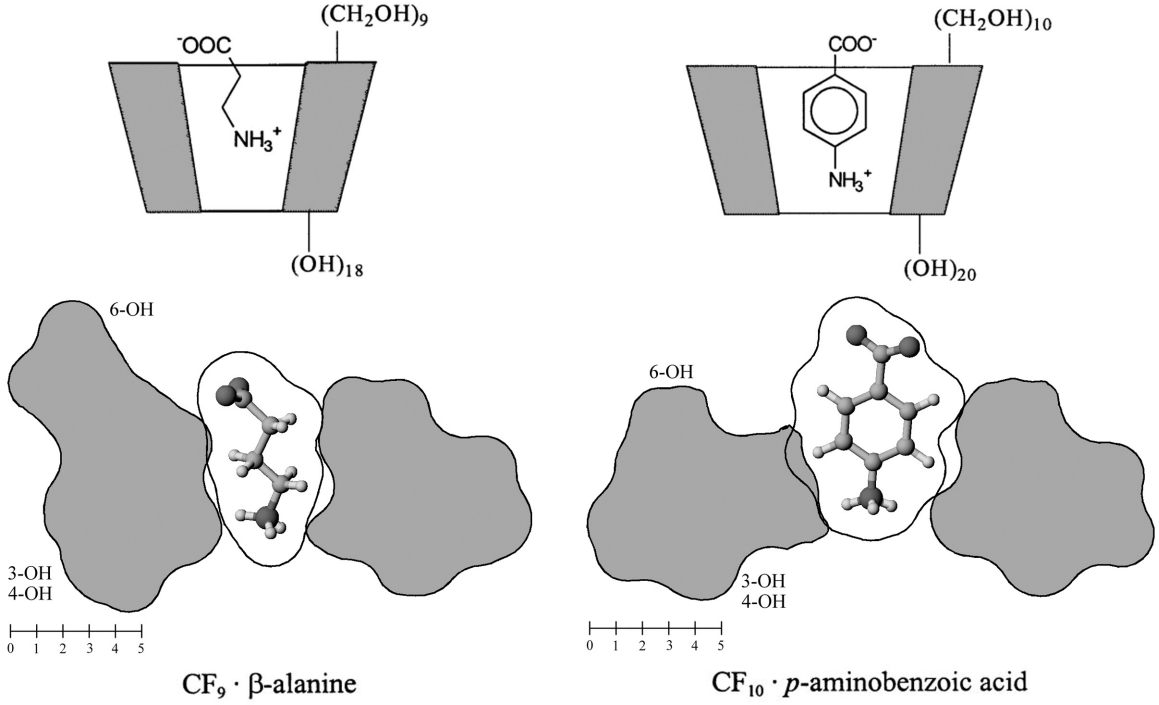

Fig. 8. Surface cross section cuts through the global energy-minimum structures of the inclusion complex of CF_9 with 3-amino-propionic acid (β-alanine, left) and of the CF_{10}·*p*-aminobenzoic acid adduct (right). The geometries depicted correspond to the "matched" host–guest orientations with antiparallel alignment of the dipoles and inclusion of the hydrophobic parts of the guest molecule in the respective cavities. The irregular shape of the cyclofructin surface cross-section cuts is related to the alternating "*inward*/*outward*" inclination of the fructofuranose residues. Whilst the CF_9 cavity and the zigzag-chain of β-alanine result in a nearly perfect steric fit, CF_{10} requires elliptic distortion to accommodate the disk-shaped aromatic guest.

host and guest dipoles. Indeed, β-alanine proves to be an essentially perfect steric fit for CF_9, the hydrophobic parts of the *all-trans*, zigzag arranged aliphatic spacer fully penetrate the cylindrical cavity and fixing the charged hydrophilic head groups at both ends, i.e., the guest's carboxylate group close to the 6-CH_2OH side of the macrocycle, and the amino function at the other, close to

the 3-OH/4-OH groups. Correspondingly, *p*-aminobenzoic acid "matches" the steric as well as electrostatic features of CF_{10}, whereby an "*induced-fit*" type mechanism [45] describes the formation of the complex in a more realistic way than the static "*lock-and-key*" concept [46]: the benzene ring is deeply incorporated into the cavity, and the host displays a pronounced elliptical distortion in order to accommodate the disk-shape of the guest.

3. Conclusion

Both the MLP and the MEP patterns clearly illustrate the crown ether-type properties of the cyclofructins **1–3** with six to eight fructose residues, with respect to capturing and complexing metal ions; the results obtained agree with experimental data, and the functional groups involved in cation complexation are identified. In relation to the inclusion complex formation of cyclodextrins that is mainly governed by hydrophobic interactions, the cyclofructins **1–3** are devoid of a central cavity, yet represent an interesting complementary example to study electrostatic interactions of carbohydrates with metal cations. The larger ring homologs, CF_9 (**4**) and CF_{10} (**5**) exhibit torus-like shape with "through-going" cavities, providing both, electrostatic complexation and hydrophobic inclusion. The computer-assisted evaluation of possible inclusion phenomena by **4** and **5** revealed both—depending on the steric complementarity of host and guest—"*lock-and-key*" as well as "*induced-fit*" type complex formation, during which the host adapts its shape in a more or less pronounced fashion to the steric requirements of the guest. Further insights into the metal cation and inclusion complexation capabilities of the cyclofructins are expected to emerge from molecular dynamics simulations in water, which are to be reported in due course. In the case of CF_6, an 750 ps MD simulation in a box of 606 water molecules has already been performed [47], showing its solute conformation to be very similar to the calculated in vacuo energy-minimum geometry of Fig. 2.

4. Experimental

Solid-state structure of α-cyclofructin CF_6, (**1**).—The atomic coordinates of the CF_6-trihydrate solid-state geometry [21] ($C_{36}H_{60}O_{30}\cdot 3\ H_2O$) were retrieved from the Cambridge Crystallographic Data File [48] (CCDF-Refcode VIPRAN10, space group $R3$, $Z=3$), missing hydrogen atoms in the structure determination were geometrically repositioned, the water of crystallization was removed; all molecular parameters listed in Table 1 were recalculated from this data set.

Force-field calculations.—All molecular geometry calculations are based on the PIMM91 force-field program [24]; structures were fully energy-optimized without any geometry restraints for in vacuo conditions ($\varepsilon = 1.0$), with a convergence criterion of root-mean-square deviations of the gradients of less than 5.0×10^{-4} eV/Å.

Mode of generation of cyclofructin start structures.—For **1–5**, in each case, two C_n symmetrical starting structures were generated by *n*-fold assembly of each of the two crystallographically independent fructofuranose geometries contained in the asymmetric unit of the crystal structure of CF_6 (**1**), both in $^4T_3$ conformations with Θ (O-1–C-1–C-2–O-1′) torsion angles of $\Theta_1 = 163.4°$ and $\Theta_2 = 52.3°$, respectively. Fitting of the O-1 atoms to form regular propeller-type anellated *n*-polygons was performed via a rigid body rotation and fitting procedure [49,50]. Analogous fitting of the asymmetric disaccharide unit Fru*f*-β-(1→2)-Fru*f* yielded $C_{n/2}$ symmetrical starting structures for the even-membered cyclofructins **1, 3**, and **5**, with *n*/2-polygons formed by the O-1/O-1″ atoms; for the odd-membered CF_7 (**2**) and CF_9 (**4**), a fructofuranose of either type was added as the remaining last unit. After geometrically repositioning all CH and OH hydrogens, all structures were fully energy-optimized and entered into Monte Carlo (MC), and "*random-walk*" conformational analysis procedures.

Monte Carlo (MC) and "random-walk" *simulations.*—All structure manipulations were performed through external computer programs [50], by which PIMM91 was controlled and used for the energy-optimizations only. Geometry variations of the cyclofructins **1–5** involved re-setting all freely rotatable 4*n exocyclic* torsion angles (H-3–C-3–O-3–H, H-4–C-4–O-4–H, C-5–C-6–O-6–H, and ω, i.e., O-5–C-5–C-6–O-6) to random values in each simulation step. To simultaneously vary the furanose ring conformations as well as the cyclofructin backbones, one or two "*corner-flap angles*" [26] out of a total of 8*n* parameters (five furanose ring torsions and three intersaccharidic dihedrals

per monosaccharide residue) were randomly altered; the adjacent *endocyclic* ring torsion angles and the positions of the substituents were adjusted accordingly to diminish steric overlaps. All newly generated conformations were fully energy-minimized (PIMM91); during the "*random-walk*" simulations the resulting conformations were accepted in any case as the starting structures for the next computational cycle; in the Monte-Carlo runs, structures were accepted according to the standard energy–weighted scheme [25]. In all cases, MC calculations and the "*random-walks*" yielded converging molecular conformations and energies (total number of optimized structures for CF_6 (**1**): 135 890, CF_7 (**2**): 136 961, CF_8 (**3**): 109 237, CF_9 (**4**): 86 281, and CF_{10} (**5**): 84 654).

Molecular surfaces, molecular lipophilicity patterns (MLPs), and electrostatic potential profiles (MEPs).—Calculation of the molecular contact surfaces, MLPs, and MEPs (using the PIMM91 atomic charges) was carried out by using the MOLCAD [28,38,39] molecular modeling program (Fig. 6). Surfaces for the inclusion complexes were generated for the guest and host molecules separately, and subsequently reassembled to the complex. Cross-cut plots were computed from the intersection of a plane with the molecular surfaces [50]; all black–and-white molecular plots were generated using the MolArch$^+$ program [50]. Visualization of the MEP and MLP surface qualities was done with MOLCAD [28] by color-coded projection of the computed values onto these surfaces applying texture mapping [39]. Scaling of the molecular hydrophobicity patterns and electrostatic potential profiles was performed in relative terms for each molecule separately, and no absolute values are displayed.

Iso-energy contour surfaces.—The iso-energy contour surfaces for the interaction of the cyclofructins **1–5** with charged probe spheres were generated by superimposing a three–dimensional grid of 0.25 Å step size to each cyclofructin [50]. For each grid point, the interaction energy of the cyclofructin with a proton (H^+), or alternatively for a chloride ion (Cl^-), was calculated by considering the sum of electrostatic and van der Waals energy terms [50]; energy terms were used as implemented in the PIMM91 force-field program [24]: electrostatics are computed using the PIMM91 partial atomic charges of the fully energy–optimized structures and Ohno–Klopman-type distance dependencies. All atomic interaction parameters, as well as the van der Waals energy terms (mixed exponential and 12-6-terms) were extracted from the PIMM91 force-field [24].

Cyclofructin inclusion complexes.—Start structures of the inclusion complexes of CF_9 (**4**) with 3-aminopropionic acid ($C_{54}H_{90}O_{45}\cdot C_3H_7O_2N$) and of CF_{10} (**5**) with *p*-aminobenzoic acid ($C_{60}H_{100}O_{50}\cdot C_7H_7O_2N$) were generated with either host–guest alignment and geometry optimized (PIMM91). MD simulations (timestep 1 fs, $T = 300$ K) of 25 ps length were performed for each complex, structures were saved every 25 fs. Subsequently, all complex geometries obtained (1000 configurations each) were fully energy-minimized; the global energy-minimum conformations are depicted in Fig. 8.

Acknowledgements

We thank Professor Dr. J. Brickmann, Institut für Physikalische Chemie, Technische Universität Darmstadt, for providing us with the MOLCAD molecular modeling software package, and Professor Dr. H.J. Lindner for access to the PIMM91 source code.

References

[1] S. Immel, G.E. Schmitt, and F.W. Lichtenthaler, in J.J. Torres Labandeira (Ed.), Proceedings 9th Internat. Cyclodextrin Symp., Kluwer Academic, Dordrecht, The Netherlands, in press.
[2] M. Kawamura and T. Uchiyama, *Carbohydr. Res.*, 260 (1994) 297–304.
[3] M. Kawamura, T. Uchiyama, T. Kuramoto, Y. Tamura, and K. Mizutani, *Carbohydr. Res.*, 192 (1989) 83–90.
[4] T. Uchiyama, *Inulin and Inulin-Containing Crops*, Elsevier Science, Amsterdam, The Netherlands, 1993, pp. 143–148.
[5] F.W. Lichtenthaler and S. Immel, *Tetrahedron: Asymmetry*, 5 (1994) 2045–2060.
[6] S. Immel and F.W. Lichtenthaler, *Liebigs Ann. Chem.*, (1996) 39–44.
[7] T. Nakagawa, K. Ueno, M. Kashiwa, and J. Watanabe, *Tetrahedron Lett.*, 35 (1994) 1921–1924.
[8] (a) T. Takaha, M. Yanase, H. Takata, S. Okada, and S.M. Smith, *J. Biol. Chem.*, 271 (1996) 2902–2908; (b) Y. Tesada, M. Yanase, H. Takata, T. Takaha, and S. Okada, *J. Biol. Chem.*, 272 (1997) 15729–15733.
[9] S. Immel, J. Brickmann, and F.W. Lichtenthaler, *Liebigs Ann. Chem.*, (1995) 929–942.
[10] (a) T. Fujiwara, N. Tanaka, and S. Kobayashi, *Chem. Lett.*, (1990) 739–742; (b) I. Miyazawa,

T. Endo, H. Ueda, S. Kobayashi, and T. Nagai, *Eur. J. Pharm. Sci.*, 3 (1995) 153–162; (c) R. Uchida, A. Nasu, K. Tobe, T. Oguma, and N. Yamaji, *Carbohydr. Res.*, 287 (1996) 271–274.

[11] T. Endo, H. Nagase, H. Ueda, S. Kobayashi, and T. Nagai, *Chem. Pharm. Bull.*, 45 (1997) 532–536.

[12] H. Ueda, T. Endo, H. Nagase, S. Kobayashi, and T. Nagai, *J. Inclusion Phenom. Mol. Recogn. Chem.*, 25 (1996) 17–20.

[13] J. Jacob, K. Geßler, D. Hoffmann, H. Sanbe, K. Koizumi, S.M. Smith, T. Takaha, and W. Saenger, *Angew. Chem.*, 110 (1998) 626–629; *Angew. Chem. Int. Ed.*, 37 (1998) 605–609.

[14] T. Endo, H. Ueda, S. Kobayashi, and T. Nagai, *Carbohydr. Res.*, 269 (1995) 369–373.

[15] T. Endo, H. Nagase, H. Ueda, A. Shigihara, S. Kobayashi, and T. Nagai, *Chem. Pharm. Bull.*, 45 (1997) 1856–1859.

[16] H. Ueda, T. Endo, H. Nagase, S. Kobayashi, and T. Nagai, in J.J. Torres Labandeira (Ed.), Proceedings 9th Internat. Cyclodextrin Symp., Kluwer Academic, Dordrecht, The Netherlands, in press.

[17] S. Kitamura, H. Isuda, J. Shimada, T. Takada, T. Takaha, S. Okada, M. Mimura, and K. Kajiwara, *Carbohydr. Res.*, 304 (1997) 303–314.

[18] Y. Nogami, K. Nasu, T. Koga, K. Ohta, K. Fujita, S. Immel, H.J. Lindner, G.E. Schmitt, and F.W. Lichtenthaler, *Angew. Chem.*, 109 (1997) 1987–1991; *Angew. Chem. Int. Ed. Engl.*, 36 (1997) 1899–1902.

[19] K. Fujita, H. Shimada, K. Ohta, Y. Nogami, K. Nasu, and T. Koga, *Angew. Chem.*, 107 (1995) 1783–1784; *Angew. Chem. Int. Ed. Engl.*, 34 (1995) 1621–1622.

[20] Y. Nogami, K. Fujita, K. Ohta, K. Nasu, H. Shimada, C. Shinohara, and T. Koga, *J. Inclusion Phenom. Mol. Recogn. Chem.*, 25 (1996) 53–56.

[21] M. Sawada, T. Tanaka, Y. Takai, T. Hanafusa, T. Taniguchi, M. Kawamura, and T. Uchiyama, *Carbohydr. Res.*, 217 (1991) 7–17.

[22] (a) N. Yoshie, H. Hamada, S. Takada, and Y. Inoue, *Chem. Lett.*, (1993) 353–356; (b) T. Uchiyama, M. Kawamura, T. Uragami, and H. Okuno, *Carbohydr. Res.*, 241 (1993) 245–248.

[23] Y. Takai, Y. Okumura, T. Tanaka, M. Sawada, S. Takahashi, M. Shiro, M. Kawamura, and T. Uchiyama, *J. Org. Chem.*, 59 (1994) 2967–2975.

[24] (a) H.J. Lindner and M. Kroeker, PIMM91—Closed Shell PI-SCF-LCAO–MO-Molecular Mechanics Program, Darmstadt University of Technology, Germany, 1996; (b) A.E. Smith and H.J. Lindner, *J. Comput.-Aided Mol. Des.*, 5 (1991) 235–262.

[25] (a) N. Metropolis, A.W. Rosenbluth, M.N. Rosenbluth, A. Teller, and E. Teller, *J. Chem. Phys.*, 21 (1953) 1087–1092; (b) W. F. van Gunsteren and H.J.C. Berendsen, *Angew. Chem.*, 102 (1990) 1020–1050; *Angew. Chem. Int. Ed. Engl.*, 29 (1990) 992–1023.

[26] H. Goto and E. Osawa, *J. Am. Chem. Soc.*, 111 (1989) 8950–8951.

[27] The 3D-structures can be viewed at:http://caramel.oc.chemie.tu-darmstadt.de/immel/3Dstructures.html; MOLCAD graphics are available at: http://caramel.oc.chemie.tu-darmstadt.de/immel/molcad/gallery.html.

[28] (a) J. Brickmann, *MOLCAD—MOLecular Computer Aided Design*, Darmstadt University of Technology, Germany, 1996; *J. Chim. Phys.*, 89 (1992) 1709–1721; (b) M. Waldherr-Teschner, T. Goetze, W. Heiden, M. Knoblauch, H. Vollhardt, and J. Brickmann, in F.H. Post and A.J.S. Hin (Eds.), *Advances in Scientific Visualization*, Springer, Heidelberg, Germany, 1992, pp. 58–67; (c) J. Brickmann, T. Goetze, W. Heiden, G. Moeckel, S. Reiling, H. Vollhardt, and C.-D. Zachmann, in J.E. Bowie (Ed.), *Insight and Innovation in Data Visualization*, Manning, Greenwich, U.K., 1994, pp. 83–97.

[29] (a) F.M. Richards, *Ann. Rev. Biophys. Bioeng.*, 6 (1977) 151–176; *Carlsberg. Res. Commun.*, 44 (1979) 47–63; (b) M.L. Connolly, *J. Appl. Cryst.*, 16 (1983) 548–558; *Science*, 221 (1983) 709–713.

[30] B. Lee and F.M. Richards, *J. Mol. Biol.*, 55 (1971) 379–400.

[31] (a) D. Cremer and J.A. Pople, *J. Am. Chem. Soc.*, 97 (1975) 1354–1358; (b) G.A. Jeffrey and R. Taylor, *Carbohydr. Res.*, 81 (1980) 182–183.

[32] J.E. Kilpatrick, K.E. Pitzer, and R. Spitzer, *J. Am. Chem. Soc.*, 69 (1947) 2483–2488.

[33] (a) J.D. Dunitz and P. Seiler, *Acta Crystallogr., Sect. B*, 30 (1974) 2339–2341; (b) E. Maverick, P. Seiler, B. Schweizer, and J.D. Dunitz, *Acta Crystallogr., Sect. B*, 36 (1980) 615–620.

[34] (a) C.J. Pedersen, *J. Am. Chem. Soc.*, 89 (1967) 2495–2496; 7017-7036; (b) J.W.H.M. Uiterwijk, S. Harkema, and D. Feil, *J. Chem. Soc., Perkin Trans. 2*, (1987) 721–731.

[35] F.W. Lichtenthaler and S. Immel, *Liebigs Ann. Chem.*, (1996) 27–37.

[36] R.J. Clarke, J.H. Coates, and S.F. Lincoln, *Adv. Carbohydr. Chem. Biochem.*, 46 (1988) 205–249.

[37] W. Blokzijl and J.B.F.N. Engberts, *Angew. Chem.*, 105 (1993) 1610–1648; *Angew. Chem. Int. Ed. Engl.*, 32 (1993) 1545–1579.

[38] W. Heiden, G. Moeckel, and J. Brickmann, *J. Comput.-Aided Mol. Des.*, 7 (1993) 503–514.

[39] M. Teschner, C. Henn, H. Vollhardt, S. Reiling, and J. Brickmann, *J. Mol. Graphics*, 7 (1994) 98–105.

[40] F.W. Lichtenthaler and S. Immel, in M. Mathlouthi, J.A. Kanters, and G.G. Birch (Eds.), *Sweet Taste Chemoreception*, Elsevier Applied Science, London/New York, 1993, pp. 21–53.

[41] F.W. Lichtenthaler and S. Immel, *Internat. Sugar J.*, 97 (1995) 12–22.
[42] F.W. Lichtenthaler and S. Immel, *Starch/Stärke*, 48 (1996) 145–154.
[43] F.W. Lichtenthaler and S. Immel, in J. Szejtli and L. Szente (Eds.), *Proc. 8th Internat. Symp. on Cyclodextrins*, Kluwer Academic, Dordrecht, The Netherlands, 1996, pp. 3–16; *J. Inclusion Phenom. Mol. Recognit. Chem.*, 25 (1996) 3–16.
[44] H. Gohlke, S. Immel, F.W. Lichtenthaler, and G.E. Schmitt in J.J. Torres Labandeira (Ed.), *Proc. 9th Internat. Symp. on Cyclodextrins*, Kluwer Academic, Dordrecht, The Netherlands, in press.
[45] D.E. Koshland, Jr., *Angew. Chem.* 106 (1994) 2468–2471; *Angew. Chem. Int. Ed.*, 33 (1994) 2408–2412.
[46] (a) E. Fischer, *Ber. Dtsch. Chem. Ges.*, 27 (1894) 2985–2993; (b) F.W. Lichtenthaler, *Angew. Chem.*, 106 (1994) 2456–2467; *Angew. Chem. Int. Ed. Engl.*, 33 (1994) 2364–2374.
[47] S. Immel, G.E. Schmitt, and F.W. Lichtenthaler, in J.J. Torres Labandeira (Ed.), *Proceedings 9th Internat. Cyclodextrin Symp.*, Kluwer Academic, Dordrecht, The Netherlands, in press.
[48] (a) *Cambridge Crystallographic Data File*, Version 5.09, 1995; (b) F.H. Allen, S.A. Bellard, M.D. Brice, B.A. Cartwright, A. Doubleday, H. Higgs, T. Hummelink, B.G. Hummelink-Peters, O. Kennard, W.D.S. Motherwell, J.R. Rodgers, and D.G. Watson, *Acta Crystallogr., Sect. B*, 35 (1979) 2331–2339; (c) F.H. Allen, O. Kennard, and R. Taylor, *Acc. Chem. Res.*, 16 (1983) 146–153.
[49] D.J. Heisterberg, *QTRFIT—Rigid Body Rotation and Fitting Program*, The Ohio Supercomputer Center, Columbus, Ohio 43212, 1991.
[50] S. Immel, *MolArch$^+$—MOLecular ARCHitecure Modeling Program*, Darmstadt University of Technology, Germany, 1997.